Vehicle System Dynamics
Vol. 00, No. 00, Month 200x, 1–17

RESEARCH ARTICLE

Comparing Rear Wheel Steering and Rear Active Differential approaches to vehicle yaw control

M. Canale[a]* and L. Fagiano[a]

[a]*Dipartimento di Automatica e Informatica, Politecnico di Torino*
Corso Duca degli Abruzzi 24, 10129 Torino, Italy
(*Received 00 Month 200x; final version received 00 Month 200x*)

A comparison between two different approaches to vehicle stability control is carried out, employing a robust non parametric technique in the controller design. In particular, an enhanced Internal Model Control strategy, together with a feedforward action and a suitably generated reference map, is employed for the control of a vehicle equipped either with a Rear Wheel Steering (RWS) system or with a Rear Active Differential (RAD) device. The uncertainty arising from the wide range of operating conditions is described by an additive model set employed in the controller design. Extensive steady state and transient tests simulated with an accurate 14 degrees of freedom nonlinear model of the considered vehicle show that both systems are able to improve handling and safety in normal driving conditions. RAD devices can make the vehicle reach higher lateral acceleration values but they achieve only slight stability improvements against oversteer. On the other hand, 4WS systems can greatly improve both vehicle safety and maneuverability in all driving situations, making this device an interesting and powerful stability system.

Keywords: vehicle yaw control; vehicle stability control; rear active differential; rear wheel steering

1. Introduction

The development of active systems for vehicle stability gave rise to significant improvements in driving safety as well as handling and comfort characteristics. In this context, different solutions have been proposed in terms of employed actuators and control algorithms, and the topic is still an object of intense research activities from both industrial and academic sides (see e.g. [1–12]). In order to impose a desired car behaviour, the existing strategies modify the vehicle dynamics exploiting as *physical mechanisms* (or *input channels*) either appropriate distributions of longitudinal tyre forces or active front/rear wheel steering angles. Most systems rely on different left–right distribution of longitudinal forces to generate an equivalent yaw moment applied to the vehicle. For example, active braking actions are employed in VDC (Vehicle Dynamic Control) and ESP (Electronic Stability Program) systems (see e.g. [1, 2]), while active differential devices employ appropriate traction force combinations (see e.g. [3–5]). Other systems, like active front steering and four wheel steer by wire, exploit the superimposition of front and/or rear steering angles to modify the vehicle dynamics (see e.g. [6–12]). Indeed, any active stability device is able to influence vehicle dynamics up to a physical limit, which depends on the tyre and suspension system and on the road characteristics. Inside this limit, however, different performance can be obtained by stability systems which employ different physical mechanisms and, in general, some input channels may be more effective than others to improve the stability of normal passenger cars. In this context, this paper aims

*Corresponding author. Email: massimo.canale@polito.it

ISSN: 0042-3114 print/ISSN 1744-5159 online

DOI: 10.1080/0042311YYxxxxxxxx
http://www.informaworld.com

to make a comparative study over the performance obtained by two active stability systems, both acting at the rear axle, which employ different input channels. In particular, a Rear Active Differential (RAD) and a Rear Wheel Steer by wire system (RWS) have been chosen as active devices. Such a comparison is motivated by observing that, contrary to systems that use braking actions, as a first approximation both these devices avoid to reduce the vehicle speed to keep system safety, thus they are also suitable to be employed in normal driving situations, to enhance the vehicle maneuverability (see e.g. [4]). A yaw rate feedback has been adopted in both systems, as it is usually done in most active stability devices. **Moreover, since the vehicle operates under a wide range of speed, load and friction situations, causing uncertainty in the dynamic modeling, safety (i.e. stability) has to be robustly guaranteed by the control system. Several robust approaches to active vehicle control have been introduced in the relevant literature. In particular, both linear and nonlinear model based solutions have been proposed using either parametric or non parametric uncertainty descriptions. For example, in [7] and [13], robust sliding mode techniques have been employed respectively in parametric and non parametric settings. Linear methodologies have been considered in [12] where parametric uncertainty and a two degrees of freedom structure has been implemented through speed dependent gain scheduling and in [4, 11] where IMC controllers have been designed in the presence of unstructured uncertainty. Besides robustness, another important issue to be taken into account is the saturation of the control input arising from the physical limitations of the actuation device. In this context, the use of (nonlinear) MPC control laws (see e.g. [14] and [15]) or the inclusion of anti–windup structures in the implementation of linear controllers (see e.g. [4, 10]) guarantee stability in the presence of control input saturation, and robustness properties are checked a posteriori. Therefore, the control designer has to take care of both robust stability and input saturation aspects. In order to take into account such issues,** in this paper Internal Model Control (IMC) techniques are used in the design of the feedback controller, as they are well established control methodologies able to handle effectively both robustness (see [16]) and saturation (see e.g. [17, 18]) issues. In particular, the enhanced IMC structure presented in [19], which guarantees robust stability as well as improved performance during saturation, will be employed. As such design methodology is based on robust H_∞ optimization techniques, a linear model of the vehicle dynamics will be considered and an unstructured uncertainty description approach will be adopted to take into account the different operating conditions of the vehicle. In addition, a feedforward contribution is used to enhance system performance in the transient phase. To show in a realistic way the results of the proposed comparative study, tests will be performed using a detailed nonlinear 14 degrees of freedom vehicle model of a prototype Alfa Romeo segment E car which proved to give accurate simulation results as compared with real vehicle acquired data. The paper is organized as follows. In Section 2 problem settings and control requirements are introduced. Vehicle modeling issues are presented in Section 3 while the adopted control structure and the related design principles are described in Section 4. Finally, in Section 5, extensive simulation studies are reported in order to compare the behaviour of RAD and RWS systems under a wide range of driving scenarios.

2. Problem formulation

The objective of this paper is to compare two approaches for vehicle stability control, which employ different physical mechanisms to enhance safety and handling. RAD devices are able to influence the vehicle motion by properly distributing traction forces between left and right rear wheels, thus generating suitable yaw moments. In particular, the full active RAD [20] considered in this paper is the same of [4]: such a system, composed

of two clutches and their electro–hydraulic actuators applied on the rear driveshafts, is able to transfer driving torque from one rear wheel to the other, independently from their relative speed (except for very narrow turns at low speed). The effect of the consequent left–right torque distribution can be regarded as a yaw moment acting on the vehicle, whose limits of ± 2500 Nm are due to the maximum pressure value that the valves can handle (i.e. 30 bar). Note that, for structural safety reasons, the clutches cannot be activated together at the same time, moreover for any given vehicle operating condition, a positive/negative yaw moment can be univocally obtained by actuating the lef/right clutch. Thus, for control design in the case of RAD, a single manipulated variable can be considered, i.e. a yaw moment M_z acting on the vehicle center of gravity (c.o.g.), with a saturation value of 2500 Nm. A valve actuation logic is then employed to convert the control input into input current for the left or right valve.

Rear Wheel Steering systems use a completely different mechanism to influence the vehicle dynamics, since they rely on actuators able to change the steering angles of the rear wheels. In this case, the maximum allowable rear steering angles are restricted due to space constraints: in this paper the limit values of $\pm 5^\circ$ are considered (see e.g. [10]). The left and right rear steering angles have to be similar and, in general, they can be positive or negative without regards for the vehicle motion conditions. Thus, control design for the RWS system can be carried out considering as single input variable the steering angle δ_r of the rear wheels, with a saturation value of 5°.

The IMC scheme employed in this paper is able to effectively handle the presence of actuation delays and non-ideal dynamics (see [4, 11]), however note that, apart from the saturation, the actuators considered in this work are supposed to be ideal, i.e. their dynamical properties are neglected with respect to vehicle lateral dynamics. This is motivated by the fact that the aim of this paper is to compare the performance obtained using two different kinds of dynamic action to modify the system dynamics (i.e. left/right rear traction torque distribution or rear wheel steering), without addressing the issues related to the actuation systems which, in general, can be made more responsive with increased cost.

In order to better introduce the control objectives, some notions of vehicle lateral dynamics are now recalled. The vehicle inputs are either M_z or δ_r, used for control purposes, and the front steering angle δ imposed by the driver, while the controlled variable is the vehicle yaw rate $\dot{\psi}(t)$. A quite common way to characterize the steady state vehicle handling at a given speed v is the *steering diagram* (see Figure 1, dotted line), where the front steering angle is reported with respect to the lateral acceleration a_y. The steering diagram slope at low acceleration values is a measure of the car maneuverability: the lower this value, the higher the lateral acceleration reached by the vehicle with the same front steering angle, the more the sport feeling and handling quality perceived by the driver (see e.g. [21]). At high acceleration, the course becomes nonlinear showing a saturation value that is the highest lateral acceleration the vehicle can reach. Control of rear steering wheels or active differential device can be employed to vary, under the same front steering conditions, the behaviour of a_y, modifying the slope of the steering diagram according to some desired requirements. Thus, an improved steering diagram (see Figure 1, solid line) can be introduced to define the target performance for the controlled vehicle: recalling that in steady state $a_y(t) \approx v\dot{\psi}(t)$, such an improved steering diagram can be used to compute the reference yaw rate values for the control system. More details about the design of such target curves will be reported in Section 4. Another aim of active stability systems is to achieve good damping and readiness properties during transients. This can be taken into account by the feedback design, imposing well damped closed loop characteristics, and by means of a feedforward action based on the driver input (i.e. δ) to increase system readiness. Safety (i.e. stability) requirements in the presence of the uncertainty arising from the wide range of the vehicle operating conditions can be achieved by a robust controller design, using an appropriate description of the uncertainty as it will be showed in Sections 3

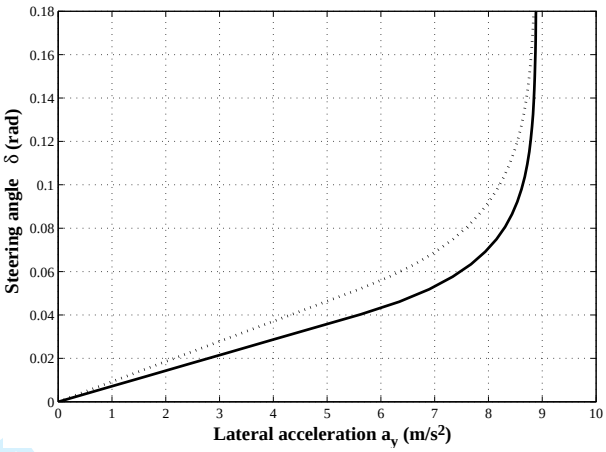

Figure 1. Uncontrolled vehicle (dotted), and target (solid) steering diagrams. Vehicle speed: 80 km/h

and 4. Moreover, the controller structure should be provided with suitable implementation solutions like anti-windup schemes to improve the system performance during saturation of the control variable.

3. Model description

A single track vehicle model (see e.g. [22]) has been used to describe the vehicle dynamics for control design purposes. Such a model is based on the following hypothesis:

- Flat road.
- Longitudinal motion resistances are ignored compared to wheel lateral forces.
- Self aligning wheel moments are ignored.
- Steering angle and vehicle side slip angle are small enough to linearize their trigonometrical functions.
- Vehicle speed is a known parameter, vehicle longitudinal acceleration is low or equal to zero.

Tyre lateral force-slip angle linear dependence is obtained by linearizing Pacejika formulation, with tyre lateral slip angle near to zero. The dynamic generation mechanisms of front and rear tyre forces are also modelled as first–order systems, by introducing the tyre lateral relaxation lengths. The model equations are the following:

$$\begin{aligned} &mv(t)\dot{\beta}(t) + mv(t)\dot{\psi}(t) = F_{yf,p}(t) + F_{yr,p}(t) \\ &J_z\ddot{\psi}(t) = aF_{yf,p}(t) - bF_{yr,p}(t) + M_z \\ &F_{yf,p}(t) + l_f/v(t)\dot{F}_{yf,p}(t) = -c_f(\beta(t) + a\dot{\psi}(t)/v(t) - \delta(t)) \\ &F_{yr,p}(t) + l_r/v(t)\dot{F}_{yr,p}(t) = -c_r(\beta(t) - b\dot{\psi}(t)/v(t) - \delta_r(t)) \end{aligned} \tag{1}$$

where β is the side-slip angle, m is the vehicle mass, J_z is the moment of inertia around the vertical axis, l is the wheel base, a and b are the distances between the center of gravity and the front and rear axles respectively; the front and rear tyre relaxation lengths are indicated as l_f and l_r, while the symbols c_f and c_r stand for the front and rear axle cornering stiffnesses. $F_{yf,p}$ and $F_{yr,p}$ are the front and rear axle lateral forces, δ_r is the rear steering angle and M_z is the external yaw moment applied to the vehicle center of gravity. Applying the Laplace transform to equations (1), the vehicle yaw rate dynamics

can be described by the following relations in the Laplace domain:

$$\dot{\psi}(s) = G_{\delta}(s)\delta(s) + G_{\delta_r}(s)\delta_r(s) \quad \text{for RWS} \tag{2a}$$

$$\dot{\psi}(s) = G_{\delta}(s)\delta(s) + G_{M_z}(s)M_z(s) \quad \text{for RAD} \tag{2b}$$

Where $G_{\delta}(s)$, $G_{\delta_r}(s)$ are the 4$^{\text{th}}$ order transfer functions between front steering angle and yaw rate and rear steering angle and yaw rate respectively, and $G_{M_z}(s)$ is the 4$^{\text{th}}$ order transfer function between yaw moment and yaw rate. Transfer functions $G_{\delta_r}(s)$ and $G_{M_z}(s)$ will be used in the design of the feedback controller for the RWS and for the RAD respectively. As already remarked, the real vehicle behaviour is influenced by several different factors that introduce model uncertainty. Therefore, to perform a robust design, an additive uncertainty linear model set of the form (3) has been employed in the control design:

$$\mathcal{G}(G,\Gamma) = \{(G(s) + \Delta(s)) : |\Delta(\omega)| \leq \Gamma(\omega)\} \tag{3}$$

where $G(s)$ is the nominal transfer function between the control variable (i.e. either δ_r or M_z) and the vehicle yaw rate, $\Delta(s)$ is the unstructured additive uncertainty (see [23]) and $\Gamma(\omega)$ is an upper bound of the magnitude of $\Delta(s)$. The generic model set $\mathcal{G}(G,\Gamma)$ yields the following two model sets in case of RWS and RAD:

$$\begin{aligned} \mathcal{G}_{\delta_r}(G_{\delta_r},\Gamma_{\delta_r}) &= \{(G_{\delta_r}(s) + \Delta_{\delta_r}(s)) : |\Delta_{\delta_r}(\omega)| \leq \Gamma_{\delta_r}(\omega)\} \\ \mathcal{G}_{M_z}(G_{M_z},\Gamma_{M_z}) &= \{(G_{M_z}(s) + \Delta_{M_z}(s)) : |\Delta_{M_z}(\omega)| \leq \Gamma_{M_z}(\omega)\} \end{aligned} \tag{4}$$

Such model sets have been obtained taking into account the effects of different vehicle speeds ($\pm$ 35% of the nominal value), vehicle inertial characteristics (up to $+25\%$ of the nominal mass with consequent geometrical parameters changes) and tyre relaxation lengths ($\pm$ 10% of the nominal value). Descriptions of $|\Delta_{\delta_r}(\omega)|$ and $|\Delta_{M_z}(\omega)|$ have been obtained by gridding on the considered model parameter variations (see [23]). **Note that additive uncertainty has been considered, instead of other kinds of uncertainty models (e.g. multiplicative), because it leads to a simple robust stability condition in the case of IMC structure, as it will pointed out in Section 4.2**.

4. Yaw control design

The employed control structure is depicted in Figure 2. In such a structure the desired

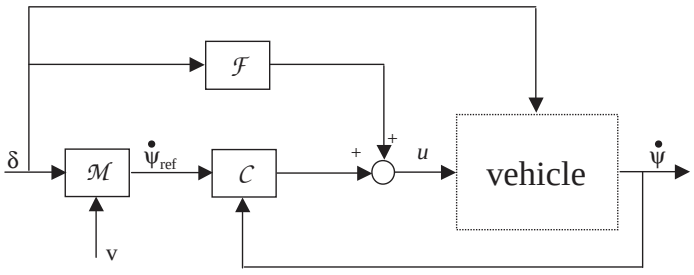

Figure 2. Overall control structure schematic.

yaw rate behaviour is imposed by the reference signal $\dot{\psi}_{\text{ref}}(t)$ generated by a static map $\mathcal{M}$ using the values of $\delta(t)$ and $v(t)$. The feedback controller $\mathcal{C}$ computes the control

contribution needed to follow the required yaw rate performance described by $\dot{\psi}_{\text{ref}}(t)$. Moreover, in order to improve the yaw rate transient response properties in face of the driver input, a feedforward control contribution $\mathcal{F}$ from $\delta(t)$ has been added too. Such a control scheme has been already employed with good results in vehicle stability control applications ([4, 11]); the design procedure will be now briefly recalled for the reader's convenience.

4.1. *Reference generator*

Reference yaw rate values are generated using a nonlinear static map

$$\dot{\psi}_{\text{ref}} = f(\delta, v) \tag{5}$$

which uses as input the front steering angle δ imposed by the driver and the vehicle speed v. The values of $f(\delta, v)$ are obtained according to the control objective, i.e. to improve the vehicle steering diagram, in terms of vehicle manoeuvrability and lateral acceleration limit, thus enhancing the overall vehicle handling quality perceived by the driver (see [21]). To compute the map values, the following single track nonlinear vehicle model, described in [4], is considered:

$$\begin{aligned} m\,v\,\dot{\psi} &= F_{yf,p}(\beta, \dot{\psi}, \delta) + F_{yr,p}(\beta, \dot{\psi}, \delta_r) \\ aF_{yf,p}(\beta, \dot{\psi}, \delta) &- bF_{yr,p}(\beta, \dot{\psi}, \delta_r) + M_z = 0 \end{aligned} \tag{6}$$

Such a model takes into account the nonlinear axle slip-lateral force relationship introduced in [24]. Numerical computation of these equations gives any feasible steady state motion condition for the nominal vehicle. In particular, equations (6) are employed in a two-step procedure. At first, they are used to compute any controlled vehicle steering diagram obtained applying every manipulated variable value inside the saturation limits of the actuators (i.e. $|\delta_r| \leq 5°$, $|M_z| \leq 2500$ Nm), within the vehicle lateral acceleration limit, for each couple of values (δ, v). Thus, for each constant speed value, the working region for the control system can be obtained (see Figure 3). This region represents a limit to the reference steering diagram that can be set for the controlled vehicle with the nominal tyre, mass and geometrical characteristics. Note that in (6) $M_z = 0$ for RWS system

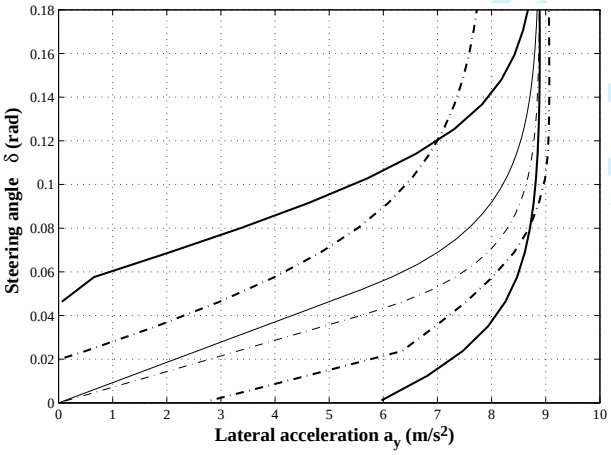

Figure 3. Control system working region, delimited by bold lines, for RWS (solid) and RAD (dash-dot) systems and uncontrolled (thin solid line) and reference (thin dashed line) vehicle steering diagrams. Speed: 100 km/h

and $\delta_r = 0$ for RAD: this characteristic leads to a difference of the potentials of the two approaches in the steady state reference choice. In fact, the analysis of Figure 3 shows that

the intervention area of RWS system is larger than that of RAD system for values of a_y up to the maximum lateral acceleration that the uncontrolled car can reach. On the other hand, RAD system is able to increase the maximum a_y value that the vehicle can reach, by better exploiting the tyre-road friction potential of the rear axle. From a practical point of view, this difference means that a RWS system is better suited to modify and improve the maneuverability of passenger cars in normal driving conditions, while a RAD can be employed to achieve the best handling performance (e.g. on sport cars), up to the physical road friction limit. Such a difference, which is independent on the control design, is due to the different physical mechanisms employed by the two approaches and their respective actuator saturation values (up to the maximum lateral acceleration limit of the vehicle).
In the second step, the reference steering diagram at each speed value is chosen within the working region according to some performance criteria (e.g. to improve the vehicle manoeuvrability by reducing the slope of the curve for small values of lateral acceleration). To this end, the steering diagram can be divided into a linear tract (i.e. small lateral acceleration values) and into a nonlinear one. In the first tract, the uncontrolled car behaviour can be expressed as:

$$\delta = \left(\frac{l}{v^2} + K_V\right) a_y = \left(\frac{l}{v} + K_V v\right) \dot{\psi} \tag{7}$$

The quantity K_V is the vehicle *understeer gradient*, which is defined as (see [22]):

$$K_V = \frac{m}{l}\left(\frac{b}{c_f} - \frac{a}{c_r}\right) \tag{8}$$

Equation (7) is obtained considering the cornering stiffness for the overall front (rear) axle instead of the single front (rear) wheels. Since the perceived handling quality of a vehicle with a lower understeer gradient is higher, reference curves in the linear tract are chosen by replacing K_V in (8) with the *desired* understeer gradient K_C such that $0 < K_C < K_V$. Then, in the nonlinear tract of the curve the desired yaw rate values are computed with a logarithmic function of δ which smoothly connects the linear tract of the curve with the chosen maximum lateral acceleration value $\bar{a}_y$ (see [4] for details). The latter is selected as the maximum lateral acceleration that the uncontrolled vehicle can reach as shown in Figure 3 (thin lines), without violating the physical upper bound suggested by [22]:

$$\bar{a}_y \leq 0.85\, g\, \mu \tag{9}$$

where μ is the available tyre-road friction and g is the gravity acceleration. Note that, as already pointed out, the active differential system would be able to increase the maximum a_y value that the vehicle can reach, however, since the aim of this paper is the comparison between the performance and robustness properties of the two control systems, the same reference values are used for both RWS and RAD. Thus, a reference understeer curve as showed in Figure 3 is computed for each couple of values of δ and v, so a map of values of $\dot{\psi}_{\text{ref}}(\delta, v)$ is obtained for each control system.

4.2. *IMC controller design*

In the present and in the following subsection the same generic symbology related to model set $\mathcal{G}$ will be used to indicate indifferently $\mathcal{G}_{M_z}$ and $\mathcal{G}_{\delta_r}$ as the design procedures are identical for both the two control strategies to be compared. In the same way, the symbol u stands for both the considered control inputs M_z and δ_r.
Internal Model Control (IMC) techniques (see [16]) based on H_∞ optimization are able

to satisfy robust stability requirements in presence of input saturation (see e.g. [19, 25]). A basic IMC structure including a model set of the form (3) is reported in Figure 4(a). However, as discussed in [18], IMC control may deteriorate the system performance when

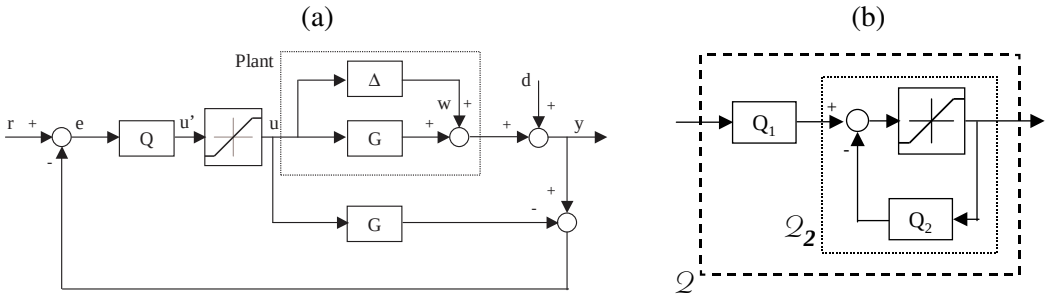

Figure 4. (a) Basic IMC scheme with model uncertainty and saturating input. (b) Nonlinear IMC enhanced controller.

saturation is active, even in absence of model uncertainty. In order to improve the performance under saturation an enhanced robust IMC structure based on the anti-windup IMC solutions presented in [18] has been proposed in [19]. In [18], the controller $Q(s)$ has been replaced by a nonlinear structure $\mathcal{Q}$ made up by the cascade connection of a linear filter $Q_1(s)$ and a nonlinear loop $\mathcal{Q}_2$, as shown in Figure 4(b).
In linear operating conditions (i.e. when the saturation is not active) the improved IMC structure is equivalent to a "standard" IMC controller of the form:

$$Q(s) = \frac{Q_1(s)}{1 + Q_2(s)} \tag{10}$$

The design procedure can be summarized in the following steps:

(1) A preliminary robust IMC controller $Q(s)$ is computed solving the following optimization problem:

$$Q(s) = \arg \min_{\|Q(s)\bar{\Gamma}(s)\|_\infty < 1} \left\| W_S^{-1}(s)\left(1 - G(s)Q(s)\right)\right\|_\infty \tag{11}$$

where $\bar{\Gamma}(s)$ is a suitable rational function with real coefficients, stable, whose magnitude strictly overbounds $\Gamma(\omega)$ and $W_S(s)$ is a weighting function introduced to take into account a desired specification on the nominal sensitivity $S(s) = 1 - G(s)Q(s)$. **The constraint $\left\|Q(s)\bar{\Gamma}(s)\right\|_\infty < 1$ accounts for robust closed loop stability in the presence of the considered additive model uncertainty, when IMC is employed**.

(2) Using controller $Q(s)$ computed in the previous step, a controller $Q_2(s)$, via the design of a preliminary filter $\bar{Q}_1(s)$, is obtained according to the criteria introduced e.g. in [17], [18]. It has to be noted that $Q_2(s)$ must ensure the stability of the non linear loop $\mathcal{Q}_2$ (see Figure 4). To this end, an upper bound $\gamma_{\mathcal{Q}_2}$ on the H_∞ norm of $\mathcal{Q}_2$ has to be computed (see [19] for details). If $\gamma_{\mathcal{Q}_2}$ is finite then the stability of $\mathcal{Q}_2$ is guaranteed. In case that the stability of $\mathcal{Q}_2$ is not assured then a new controller design has to be performed.

(3) Then, the linear controller $Q_1(s)$ can be designed by means of the following H_∞ optimization problem:

$$Q_1(s) = \arg \min_{\|Q_1(s)\bar{\Gamma}(s)\gamma_{\mathcal{Q}_2}\|_\infty < 1} \left\| W_S^{-1}(s)\left(1 - G(s)\frac{Q_1(s)}{1+Q_2(s)}\right)\right\|_\infty \tag{12}$$

4.3. *Feedforward controller design*

To improve the yaw rate transient response a further control input generated by a feedforward controller driven by the steering angle $\delta(t)$ is added. Such a feedforward yaw moment contribution is computed by means of a linear filter $F(s)$ to match the open loop yaw rate behaviour given by (2) with the one described by an objective transfer function $T_\delta^{\text{des}}(s)$:

$$\dot{\psi}(s) = T_\delta^{\text{des}}(s)\delta(s) \tag{13}$$

Thus, considering relation (2) (i.e. (2a) for RWS or (2b) for RAD) where the considered input $u(s)$ is computed as $u(s) = F(s)\delta(s)$ and $\dot{\psi}(s)$ is given by (13), the feedforward filter $F(s)$ is derived as:

$$F(s) = \frac{T_\delta^{\text{des}}(s) - G_\delta(s)}{G(s)} \tag{14}$$

Since the feedforward controller aims to enhance the transient response only, its contribution should be deactivated in steady state conditions: this is achieved when the dc-gains of $T_\delta^{\text{des}}(s)$ and $G_\delta(s)$ are the same.
Note that if such feedforward action is implemented as shown in Figure 2, the improvements introduced during saturation by the structure of Figure 4 would influence only the feedback control contribution. This may cause a slight degradation on the control performance. To avoid such a degradation, the feedforward contribution is injected at the reference level obtaining the control scheme reported in Figure 5.
In such a structure the feedforward action is realized by the linear filter $F_r(s)$, whose

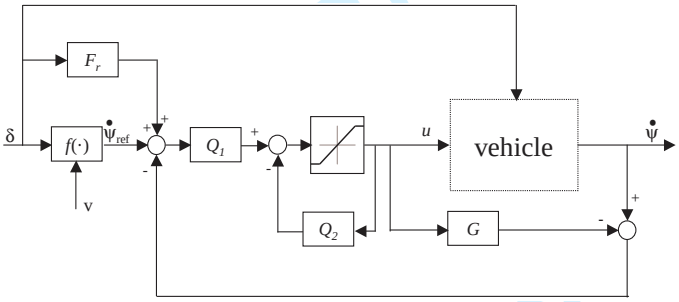

Figure 5. The employed control scheme.

expression can be computed by straightforward manipulations as:

$$F_r(s) = \left(\frac{1 + Q_2(s)}{Q_1(s)} - G(s)\right) F(s) \tag{15}$$

5. Simulation results

The control design has been performed using transfer functions $G_{\delta_r}(s)$ and $G_{M_z}(s)$ defined in (2) computed at a nominal speed $v = 100$ km/h $= 27.7$ m/s and with the following values of the other involved parameters:
$m = 1715$ kg $\quad J_z = 2690$ kgm^2 $\quad a = 1.06$ m $\quad b = 1.48$ m
$l_f = 1$ m $\quad l_r = 1$ m $\quad c_f = 89733$ Nm/rad $\quad c_r = 114100$ Nm/rad
As to the feedback controller design, the computed model uncertainties and weighting functions $\bar{\Gamma}_{\delta_r}(s)$ and $\bar{\Gamma}_{M_z}(s)$ are shown in Figure 6.

The desired performance weight to be used in the optimization problems (11) and (12) is

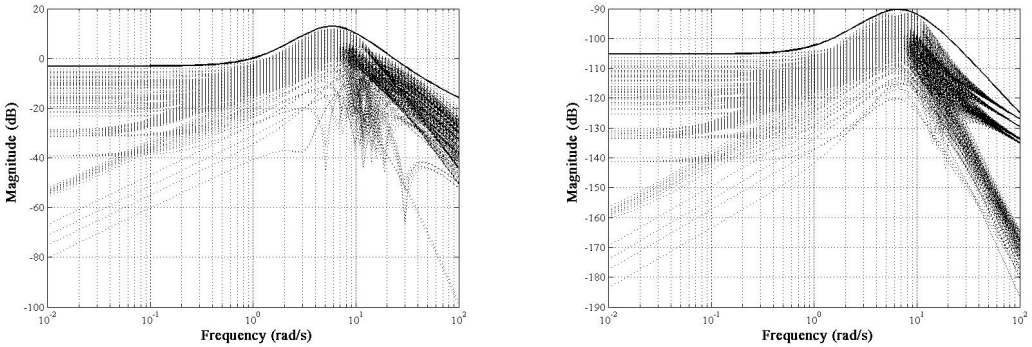

Figure 6. Left: additive uncertainty (dotted) and weighting function $|\bar{\Gamma}_{\delta_r}(j\omega)|$ (solid) for model set $\mathcal{G}_{\delta_r}$. Right: additive uncertainty (dotted) and weighting function $|\bar{\Gamma}_{M_z}(j\omega)|$ (solid) for model set $\mathcal{G}_{M_z}$.

described by the function:

$$W_{S,\delta_r}(s) = \frac{s}{s+60} \text{ for RWS}, \quad W_{S,M_z}(s) = \frac{s}{s+40} \text{ for RAD}$$

while function $T_\delta^{\text{des}}(s)$ employed for the feedforward filter design is:

$$T^{\text{des}}_{\delta,\delta_r}(s) = \frac{5}{(s+10)(s+0.5)} \text{ for RWS}, \quad T^{\text{des}}_{\delta,M_z}(s) = \frac{10}{(s+10)} \text{ for RAD}$$

Functions $W_{S,\delta_r}(s)$, $W_{S,M_z}(s)$, $T^{\text{des}}_{\delta,\delta_r}(s)$ and $T^{\text{des}}_{\delta,M_z}(s)$ **have been chosen and tuned on the basis of trial-and-error procedures, using numerical simulations, in order to achieve a good compromise between closed loop damping properties and bandwidth for each control system**.

A detailed nonlinear 14 degrees of freedom (d.o.f.) Simulink® model, **whose equations are based on [26]**, validated on the basis of real vehicle measurements, has been used to compare the performance of the vehicle equipped with RWS, the one equipped with RAD and the uncontrolled one. The model d.o.f. correspond to the standard three chassis translations and yaw, pitch, and roll angles, the four wheel angular speeds and the four wheel vertical movements with respect to the chassis. Nonlinear characteristics obtained on the basis of measurements on the real vehicle have been employed to model the tyre, steer and suspension behaviour. The employed tyre model is described e.g. in [26] and it takes into account the interaction between longitudinal and lateral slip, as well as vertical tyre load and suspension motion, to compute the tyre longitudinal and lateral forces and self–aligning moment. An example of the related tyre friction ellipses is showed in Figure 7, where the lateral friction coefficient is reported as a function of the exploited longitudinal friction (during traction) and of the tyre slip angle α. Unsymmetrical friction ellipses for traction–braking longitudinal forces is also considered. Figure 8 shows an example of comparison between the yaw rate measured on the real vehicle and the one obtained in simulation with the considered 14–d.o.f. As it can be noted, the model employed in simulation gives a good description of the vehicle dynamics as compared with real data.

The following open loop (i.e. without driver's feedback) maneuvers have been considered for simulation:

- constant speed steering pad: to evaluate steady state vehicle performance, handwheel angle is slowly increased (i.e. $1^\circ/\text{s}$) while the vehicle is moving at constant speed, until the vehicle lateral acceleration limit is reached. The considered speed values cover the

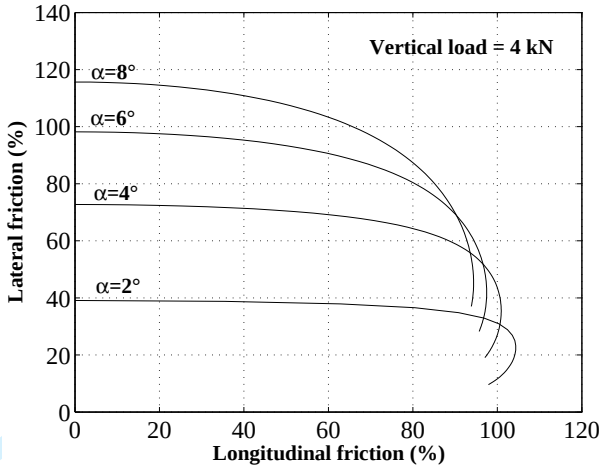

Figure 7. Front tyre friction ellipses considered in the 14 degrees of freedom model, with different values of lateral slip angle α, for a constant vertical load of 4 kN.

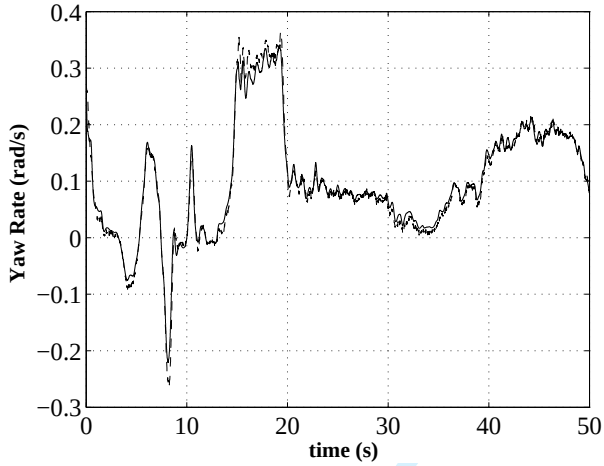

Figure 8. Comparison between the yaw rate real data (dashed) and that obtained with the 14–d.o.f. model employed for numerical simulations (solid).

range 50–130 km/h;

- steer reversal test at 100 km/h with handwheel angle of 50° and handwheel speed of 400°/s. In Figure 9(a) the employed front steering angle behaviour is showed.

- steer reversal test at 100 km/h with handwheel angle of 50° and handwheel speed of 400°/s, with decreased road friction coefficient. The considered friction coefficient is equal to 0.7 (wet road). Note that the influence of different friction coefficients has not been taken into account in the control system design, thus making this a very demanding robustness test.

- 0.7 Hz sine with dwell test. This transient maneuver is considered by NHTSA for electronic stability control evaluation (see [27, 28]), since it best excites an oversteer response from the vehicle. The front steering angle course issued during the maneuver is showed in Figure 10(a). The sine with dwell maneuver considered in [28] is performed at a starting speed of about 80 km/h (50 mph), with increasing handwheel values. To achieve a more complete analysis, in this paper the maneuver has been performed with different initial speed values and with increasing handwheel angle amplitudes, until excessive oversteer occurred (i.e. the vehicle direction 4 s after the completion of the steer input is more than 90° from the initial path, see [28]) or an handwheel angle amplitude of 330° was reached. The following quality indexes have been computed ([27, 28]):

- handwheel angle amplitude $\overline{\delta}_{SD}$ which causes excessive oversteer: the greater this quan-

tity, the better the vehicle safety characteristics

- yaw rate ratio $YRR_{1\,s} = \dot{\psi}_{1\,s}/\overline{\dot{\psi}}$ between yaw rate $\dot{\psi}_{1\,s}$ measured 1 s after maneuver completion and the maximum yaw rate $\overline{\dot{\psi}}$ which occurs in the second part of the maneuver (see Figure 10(b)): this quantity should be below 35% to attest good lateral stability
- yaw rate ratio $YRR_{1.75\,s} = \dot{\psi}_{1.7\,s}/\overline{\dot{\psi}}$ between yaw rate $\dot{\psi}_{1.7\,s}$ measured 1.7 s after maneuver completion and the maximum yaw rate $\overline{\dot{\psi}}$ which occurs in the second part of the maneuver (see Figure 10(b)): this quantity should be below 20% to attest good lateral stability
- vehicle lateral displacement $Y_{1.07\,s}$ measured 1.07 s after the beginning of the maneuver (i.e. after the second steer reversal, see Figure 10(a)): the greater this quantity, the better the vehicle responsiveness to driver input.

In order to better evaluate the system robustness in the presence of parameter variations, the steering pad and the sine with dwell maneuvers have been performed considering the nominal vehicle and a full load vehicle (+ 25% mass). Moreover, the 50° steer reversal test with high road friction has been performed in presence of lateral wind disturbance during the cornering (between 3 s and 6 s during the maneuver), with 100 km/h wind speed, and with + 20% vehicle mass. The steer reversal test has been also repeated with different values of speed and of the other main vehicle characteristics. In all the tests with increased values of mass with respect to the nominal one, the mass increments have been partitioned considering 30% of the overall increase on the front axle and 70% on the rear axle, to simulate the presence of more passengers and/or baggage. The consequent changes of inertial and geometrical vehicle characteristics have been taken into account too. The results of the performed steering pad maneuvers are

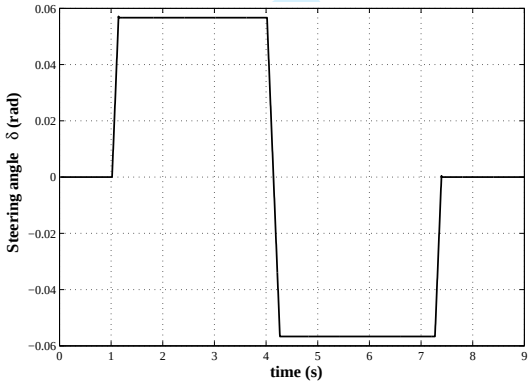

Figure 9. Front steering angle input for the steer reversal test.

reported in Table 1, in terms of understeer gradient K, maximum handwheel angle $\overline{\delta}_{\mathrm{SP}}$ and mean tracking error $\overline{e}_y$ achieved before the end of the test (i.e. vehicle instability occurred or the starting constant speed value could no longer be kept). As it was expected, the controlled vehicles show lower values of K (i.e. better handling properties), due to the imposed yaw rate reference. Moreover, the controlled vehicles have the same understeer gradient both in the nominal and in the full mass configurations, while the uncontrolled vehicle shows different values of K. The tracking error mean values are very low for both control systems in all the considered tests and configurations, showing the control system robustness under this context. As regards the maximum steering angle values before the ending of the test, in the nominal case it can be noted that while the uncontrolled and the RAD controlled vehicles show similar results, the RWS system achieves quite large $\overline{\delta}_{\mathrm{SP}}$ values, i.e. improved vehicle safety. This result is confirmed by those of the other performed tests. In the case of full load vehicle, it can be noted that the RAD system achieves

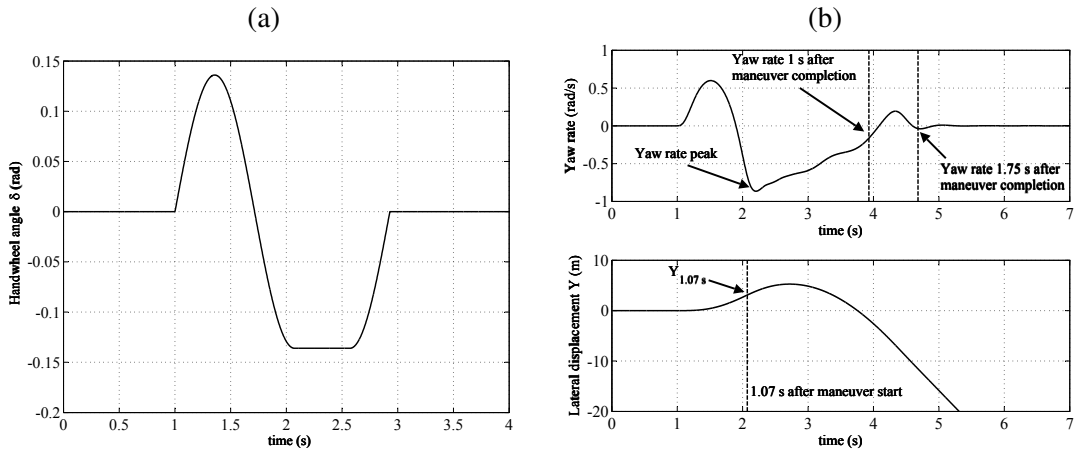

Figure 10. (a) Front steering angle input for the 0.7 Hz sine with dwell maneuver, handwheel amplitude equal to 120°. (b) Upper: typical sine with dwell yaw rate response and related measurements of yaw rate peak $\overline{\dot{\psi}}$, yaw rate $\dot{\psi}_{1\,s}$ 1 s after maneuver completion and yaw rate $\dot{\psi}_{1.75\,s}$ 1.75 s after maneuver completion. Lower: vehicle lateral displacement $Y_{1.07\,s}$ measured 1.07 s after the beginning of the maneuver

Table 1. Steering pad maneuver results: maximum handwheel angle $\overline{\delta}_{\rm SP}$, mean tracking error $\overline{e}_y$ and understeer gradient K.

	$\overline{\delta}_{\rm SP}$ (°)			$\overline{e}_y$ (rad/s)			K (m/(s^{2}rad))
	60 km/h	90 km/h	120 km/h	60 km/h	90 km/h	120 km/h	
Nominal uncontrolled vehicle	175	105	90	-	-	-	0.0047
Full load uncontrolled vehicle	114	61	35	-	-	-	0.0040
Nominal RWS vehicle	210	175	165	$2.6\,10^{-4}$	$1.8\,10^{-4}$	$1.5\,10^{-4}$	0.0039
Full load RWS vehicle	115	80	60	$3.0\,10^{-4}$	$2.8\,10^{-4}$	$2.7\,10^{-4}$	0.0039
Nominal RAD vehicle	185	105	90	$1.0\,10^{-5}$	$1.0\,10^{-6}$	$7.0\,10^{-6}$	0.0039
Full load RAD vehicle	195	120	105	$5.0\,10^{-5}$	$4.0\,10^{-6}$	$7.0\,10^{-6}$	0.0039

higher values of $\overline{\delta}_{\rm SP}$ with respect to the nominal case and also to the full load RWS vehicle. This is probably due to the increased maximum capability of the rear wheels to exchange longitudinal and lateral forces with the ground, as a consequence of the increased vertical load acting on the rear axle. However, such improvements are lost in presence of fast transient maneuvers, as it is shown by the results of the NHTSA sine with dwell test reported below. The controlled yaw rate responses during the 50° steer reversal tests at 100 km/h with lateral wind disturbance, reported in Figure 11, show the significant improvements of the system damping properties with respect to the uncontrolled vehicle. The lateral wind disturbance gives rise to undesired transient responses at 3 s and at 6 s and to a steady state error in the uncontrolled vehicle (see Figure 11), while the controlled ones show no steady state error and nearly no transient responses due to the disturbance. The courses of δ_r and M_z are shown in Figure 11 too: both control systems are able to effectively handle the saturation of the control variable. **Figure 12 shows the variation of the time responses of the controlled vehicles (either with RWS or RAD system), in terms of normalized yaw rate $\dot{\psi}(t)/\dot{\psi}_{\rm ref}(t)$ during the 50° steer reversal test, performed with varying vehicle speed between 50 km/h and 130 km/h and vehicle mass increment up to +25%. It can be noted that robust stability is achieved in both cases. The RWS system achieves a lower performance degradation with respect to the RAD, whose response is characterized by a higher overshoot in the second part of the maneuver (at about $t = 4.5$ s, see Figure 12), when vehicle oversteer is more excited. Such a difference is best highlighted by the steer reversal test performed with low road friction and by the sine with dwell maneuver.** In particular, the results of the 50° steer reversal at 100 km/h with low friction coefficient are reported in Figure 13(a). In this case the changed vehicle characteristics, which lead to an oversteering behaviour, and the low

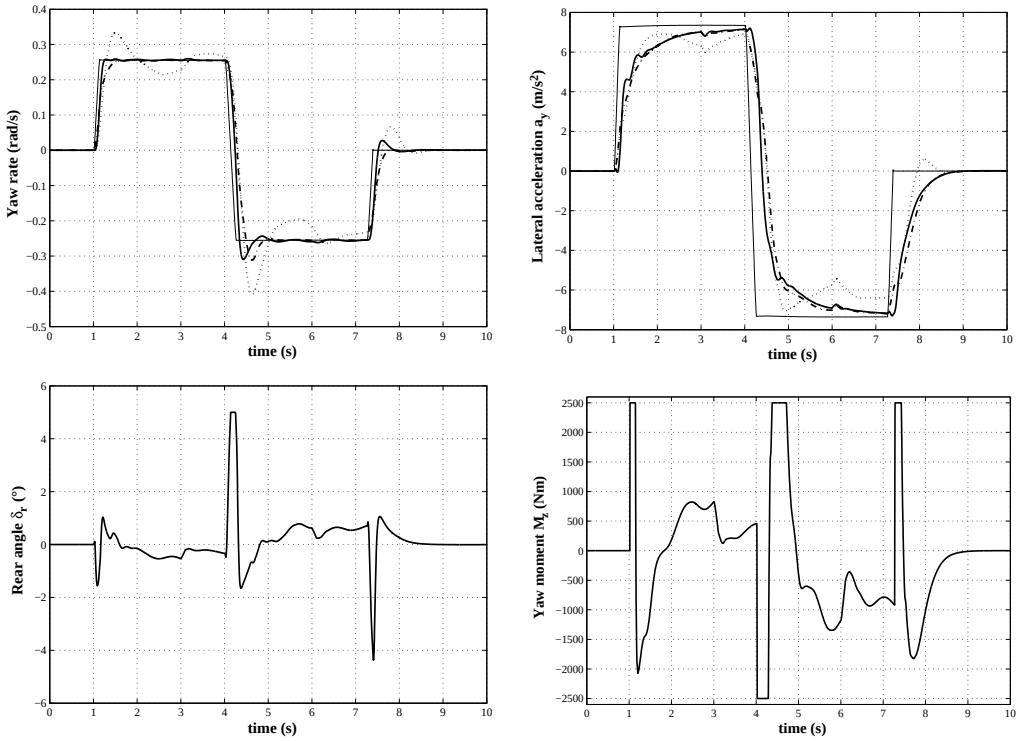

Figure 11. Steer reversal test at 100 km/h with handwheel angle value of 50°, vehicle mass increased by 20%, in presence of 100 km/h wind step disturbance between 3s and 6s. Comparison between the reference (thin solid line), uncontrolled (dotted), RWS (solid) and RAD (dash-dot) vehicle yaw rate (upper left) and lateral acceleration (upper right). Control variable behaviour for the RWS system (lower left) and for the RAD system (lower right).

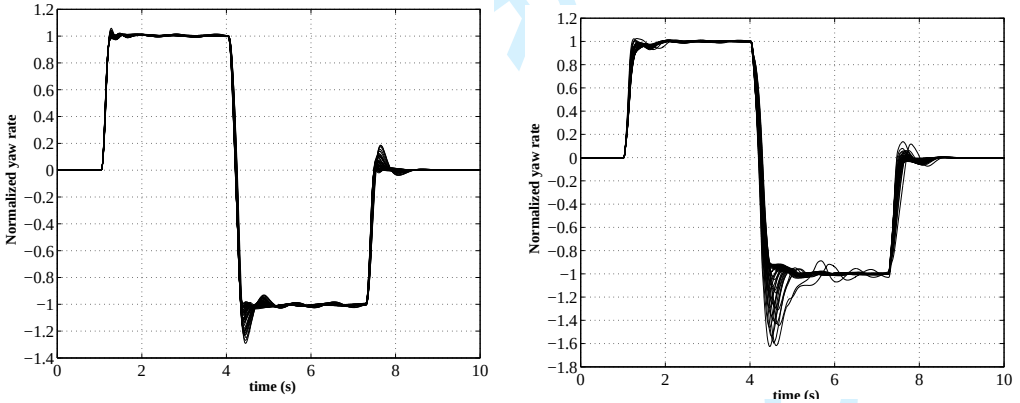

Figure 12. Steer reversal test with handwheel angle value of 50°, performed with varying vehicle speed between 50 km/h and 130 km/h and vehicle mass increment up to +25%. Courses of the normalized yaw rate $\dot{\psi}(t)/\dot{\psi}_{\text{ref}}(t)$ obtained with RWS system (left) and with RAD system (right).

road friction coefficient make the uncontrolled vehicle unstable, as shown by the vehicle yaw rate course (see Figure 13(a)). RAD system is able to keep vehicle stability for the first part of the maneuver, but instability occurs when the control action is such that the torques transmitted at each rear wheel give rise to excessive longitudinal slip values for that wheel. Longitudinal slip σ_x is defined as (see e.g. [22]):

$$\sigma_x = \begin{cases} \dfrac{r_{\text{eff}}\omega_w - v_x}{v_x} & \text{during wheel braking} \\ \dfrac{r_{\text{eff}}\omega_w - v_x}{r_{\text{eff}}\omega_w} & \text{during wheel acceleration} \end{cases} \tag{16}$$

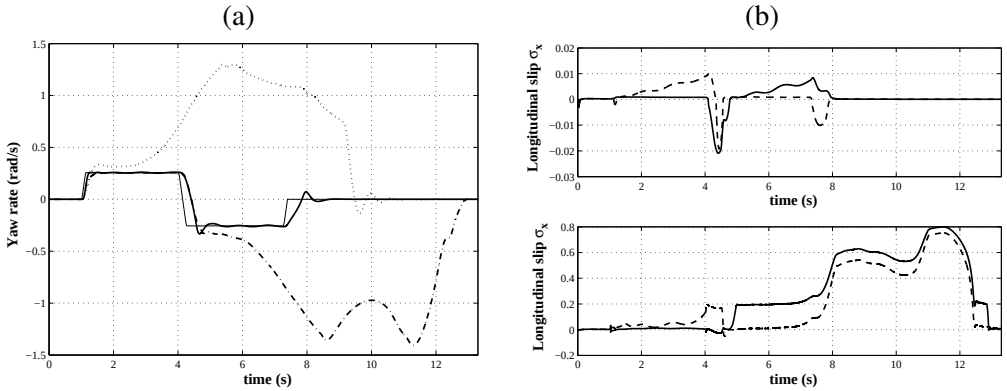

Figure 13. Steer reversal test at 100 km/h with handwheel angle value of 50°, vehicle mass increased by 20%,wet road. (a) Comparison between the reference (thin solid line), uncontrolled (dotted), RWS (solid) and RAD (dash-dot) vehicle yaw rate. (b) Comparison between left (dashed) and right (solid) rear wheel longitudinal slip for RWS (upper) and RAD (lower).

where r_{eff} is the effective tyre radius, ω_w is the wheel angular velocity and v_x is the actual longitudinal velocity at the axle of the wheel. Tyre behaviour is such that the lateral tyre force drops toward zero as the slip magnitude increases. The RAD device generates yaw moments by transferring driving torque at the rear axle from one wheel to the other, thus accelerating one wheel and braking the other. As it can be noted in Figure 13(b), during the considered maneuver, between about 4 s and 6 s, both rear wheels reach high longitudinal slip magnitude values due to the critical cornering conditions combined with the intervention of the RAD system: as a consequence, the rear axle looses its capability of generating lateral forces and instability occurs. Such a drawback, which is very likely to occur with RAD if the undertaken maneuver is such that the rear tyres work with high lateral slip angles (i.e. high lateral forces), represents a conceptual limit of the RAD device, which appears to be hardly resolvable, in a reliable and robust way, with any mechanical modification or control solution. The use of a forward active differential (FAD), acting on the torque distribution at the front wheels, would solve this problem since saturation of the front tyre forces would lead to understeer phenomena (which are less critical to be managed by the driver) rather than oversteer. Anyway, it must be remarked that the considered maneuver does not take into account any driver feedback: the fact that the RAD device is able to delay the occurrence of vehicle instability gives to the driver a higher amount of time to react in such emergency situations. On the contrary, tyre saturation phenomenon is mitigated in the RWS system (see Figure 13(b), upper), which uses rear steering instead of driving torque distribution to achieve the desired vehicle behaviour.

The handling analysis performed with the NHTSA sine with dwell maneuver confirms the reported considerations. Table 2 shows that with every considered initial speed and vehicle mass, the handwheel angle $\overline{\delta}_{\text{SD}}$ which causes excessive oversteer with the RWS controlled vehicle is much greater (more than 300% in some cases) than those of the RAD controlled and of the uncontrolled vehicles. The latter shows excessive oversteer with the lowest values of $\overline{\delta}_{\text{SD}}$, while the results obtained with the RAD system are only slightly better, with difference of about 10° for most speed values. Table 3 shows the values of $Y_{1.07\,s}$, $YRR_{1\,s}$ and $YRR_{1.75\,s}$ obtained with starting speed equal to 80 km/h (i.e. the same test considered in [28]) and handwheel amplitudes of 80°, 100° and 150°.

In some cases (e.g. full load uncontrolled vehicle with 100° handwheel angle) the values of $YRR_{1\,s}$ and $YRR_{1.75\,s}$ are not reported since excessive oversteer occurred. Note that the vehicle equipped with RAD system is slightly more responsive than the one equipped with RWS, as indicated by higher values of $Y_{1.07\,s}$, but it also has worse lateral stability properties, since the full load vehicle shows excessive oversteer with 150° handwheel angle and a yaw rate ratio $YRR_{1\,s} = 38.9\%$ with 100° handwheel angle, above the value suggested by NHTSA (35%). Thus, under this context the RAD system

Table 2. NHTSA sine with dwell maneuver: handwheel angle $\overline{\delta}_{SD}$ that causes excessive oversteer.

Vehicle speed (km/h)	60	70	80	90	100	110	120	130
Nominal uncontrolled vehicle	220°	180°	150°	130°	120°	110°	100°	90°
Nominal RWS vehicle	330°	330°	330°	330°	330°	330°	330°	330°
Nominal RAD vehicle	250°	200°	160°	140°	130°	110°	110°	100°
Full load uncontrolled vehicle	130°	110°	100°	90°	80°	70°	60°	60°
Full load RWS vehicle	290°	240°	220°	200°	190°	180°	170°	170°
Full load RAD vehicle	140°	120°	110°	100°	90°	80°	70°	70°

Table 3. NHTSA sine with dwell maneuver at 80 km/h: lateral displacement $Y_{1.07\ s}$ and yaw rate decay ratios $YRR_{1\ s}$ and $YRR_{1.75\ s}$.

	$Y_{1.07\ s}$			$YRR_{1\ s}$			$YRR_{1.75\ s}$		
Handwheel angle	80°	100°	150°	80°	100°	150°	80°	100°	150°
Nominal unc. vehicle	2.03 m	2.42 m	3.1 m	0.68%	0.86%	7.5%	0.01%	0.02%	1.60%
Full load unc. vehicle	1.94 m	2.26 m	2.81 m	1.40%	-	-	0.01%	-	-
Nominal RWS vehicle	2.04 m	2.30 m	2.9 m	0.22%	0.25%	0.28%	0.10%	0.10%	0.20%
Full load RWS vehicle	1.94 m	2.19 m	2.6 m	0.20%	0.20%	0.3%	0.10%	0.10%	0.15%
Nominal RAD vehicle	2.05 m	2.35 m	3.00 m	0.01%	0.02%	7.5%	0%	0%	0.10%
Full load RAD vehicle	1.96 m	2.23 m	2.72 m	0.70%	38.9%	-	0%	5.40%	-

can slightly improve vehicle safety with respect to the uncontrolled vehicle, but it does not appear to be suitable to correct extreme oversteering behaviours, due to the rear tyre forces saturation phenomenon which has been already put into evidence in the steer reversal test on wet road. On the other hand, the RWS controlled vehicle achieves very good results in all the considered tests, with yaw rate ratios below 0.3%, showing the control system robustness and the potentials of such a stability system to correct oversteer.

6. Conclusions

A comparative study on the use of RAD and RWS solutions to vehicle yaw control has been perfromed. Extensive steady state and transient tests simulated with an accurate model of the considered vehicle show that both systems are able to improve handling and safety in normal driving conditions. RAD devices can fully exploit tyre-road friction to reach higher lateral acceleration values but they achieve only slight stability improvements in transient maneuvers when excessive oversteer is likely to occur, due to saturation of rear tyre forces. In such maneuvers, a Forward Active Differential or a yaw control system based on braking forces (e.g. ESP or VDC) would be more appropriate for vehicle stability control because they are able to influence front tyre forces, thus correcting oversteer in the most suitable way. On the other hand, the obtained results show that the use of 4WS systems can greatly improve both vehicle safety and maneuverability in all driving situations, making this device an interesting and promising vehicle stability system.

Acknowledgements

This research was supported by funds of Ministero dell'Istruzione dell'Università e della Ricerca under the Projects "Advanced control and identification techniques for innovative applications". and "Control of advanced

References

[1] A.T.V. Zanten, R. Erhart, and G. Pfaff, *VDC, The Vehicle Dynamics Control System of Bosch*, , in *SAE Technical Paper No. 95759* , 1995.
[2] A.T.V. Zanten, *Bosch ESP Systems: 5 Years of Experience*, in *SAE Technical Paper No. 2000-01-1633*, 2000.
[3] J. Gerhard, M.C. Laiou, M. Mönnigmann, W. Marquardt, M. Lakehal-Ayat, and E.A.R. Busch, *Robust Yaw Control Design with Active Differential and Active Roll Control Systems*, in 16^{th} *IFAC World Congress*, Prague, Czech Republic, 2005.
[4] M. Canale, L. Fagiano, M. Milanese, and P. Borodani, *Robust vehicle yaw control using an active differential and IMC techniques*, Control Engineering Practice 15 (2007), pp. 923–941.
[5] F. Assadian and M. Hancock, *A Comparison of Yaw Stability Control Strategies for the Active Differential*, in *IEEE International Symposium on Industrial Electronics*, Dubrovnik, Croatia, 2005, pp. 373–378.
[6] J. Ackermann and W. Sienel, *Robust Yaw Damping of Cars with Front and Rear Wheel Steering*, IEEE Trans. on Control Systems Technology 1 (1993), pp. 15–20.
[7] J. Ackermann, J. Guldner, R. Steinhausner, and V.I. Utkin, *Linear and Nonlinear Design for Robust Automatic Steering*, IEEE Trans. on Control System Technology 3 (1995), pp. 132–143.
[8] S. Mammar and D. Koenig, *Vehicle Handling Improvement by Active Steering*, Vehicle System Dynamics 38 (2002), pp. 211–242.
[9] P. Kohen and M. Ecrick, *Active Steering - The BMW Approach Towards Modern Steering Technology*, in *SAE Technical Paper No. 2004-01-1105*, 2004.
[10] M.A. Vilaplana, O. Mason, D.J. Leith, and W.E. Leithead, *Control of Yaw Rate and Sideslip in 4-Wheel Steering Cars with Actuator Constraints*, Lecture Notes in Computer Science 3355 (2005), pp. 201–222.
[11] M. Canale and L. Fagiano, *Stability control of 4WS vehicles using robust IMC techniques*, Vehicle System Dynamics 46 (2008), pp. 911–1011.
[12] B.A. Güvenç, T. Bünte, and L. Güvenç, *Robust Two Degree-of-Freedom Vehicle Steering Controller Design*, IEEE Trans. on Control System Technology 12 (2004), pp. 627–636.
[13] M. Canale, L. Fagiano, A. Ferrara, and C. Vecchio, *Vehicle Yaw Control via Second Order Sliding Mode Control Technique*, IEEE Transactions on Industrial Electronics 55 (2008), pp. 3908–3916.
[14] M. Falcone, F. Borrelli, H.C. Tseng, and D. Hrovat, *Predictive active steering control for autonomous vehicle systems*, IEEE Transactions on Control System Technology 15 (2007), pp. 566–580.
[15] M. Canale and L. Fagiano, *Vehicle yaw control using a fast NMPC approach*, in 47^{th} *IEEE Conference on Decision and Control*, 2008.
[16] M. Morari and E. Zafiriou *Robust Process Control*, Prentice Hall, 1989.
[17] G. Goodwin, S. Graebe, and W. Levine, *Internal Model Control of Linear Systems with Saturating Actuators*, in *European Control Conference*, Gröningen, Sweden, 1993.
[18] A. Zheng, M. Kothare, and M. Morari, *Anti-Windup Design for Internal Model Control*, International Journal of Control 60 (1994), pp. 1015–1022.
[19] M. Canale, *Robust Control from Data in Presence of Input Saturation*, International Journal of Robust and Nonlinear Control 14 (2004), pp. 983–998.
[20] S. Frediani, R. Gianoglio, and F. Giuliano *System for the active control of a motor vehicle differential*, Patent no. US 2002/0016661 A1, Applicant Centro Ricerche Fiat, 2002.
[21] S. Data and F. Frigerio, *Objective Evaluation of Handling Quality*, Journal of Automobile Engineering 216 (2002), pp. 297–305.
[22] R. Rajamani *Vehicle Dynamics and Control*, Springer Verlag, 2005.
[23] S. Skogestad and I. Postlethwaite *Multivariable Feedback Control. 2^{nd} edition*, Wiley, 2005.
[24] E. Bakker, L. Lidner, and H. Pacejka, *A New Tyre Model with an Application in Vehicle Dynamics Studies*, in *SAE Paper 890087*, 1989.
[25] S. Malan, M. Milanese, D. Regruto, and M. Taragna, *Robust Control from Data Via Uncertainty Model Sets Identification*, International Journal of Robust and Nonlinear Control 14 (2004), pp. 945–958.
[26] G. Genta *Motor Vehicle Dynamics, II ed.*, World Scientific, 2003.
[27] G.J. Forkenbrock, D. Elsasser, and B. O'Hara, *NHTSA's Light Vehicle Handling and ESC Effectiveness Research Program*, ESV Paper Number 05-0221 (2005).
[28] G.J. Forkenbrock and P. Boyd, *Light Vehicle ESC Performance Test Development*, ESV Paper Number 07-0456 (2007).